Academic Journal of Science and Technology
ISSN: 2771-3032 | Vol. 14, No. 3, 2025

Inverter-based Resources for Power Generation Technology

Xinyi Wang[1, a]

[1]Faculty of Engineering, Architecture & Info Tech, The University of Queensland, Brisbane, Queensland, 4067, Australia
[a]wangxinyi200010@163.com

Abstract: The aim of this research project is to explore the possibility of maintaining the stability of frequency control in power systems today where the share of high percentage inverter resources is gradually increasing. By conducting experiments using SCADA, this research aims to find effective ways to analyze the specific generation methods and compare them with the conventional ones, and finally to explore the possibilities of maintaining the stability of the frequency of the power system in the above mentioned scenario.

Keywords: Inverter-based resources; power system frequency stability; SCADA; generation methods.

1. Introduction

With the rise of renewable energy, people are becoming more aware of the importance of sustainable development and ecological protection, especially clean energy sources such as wind and solar. These energies cannot be directly connected to the grid and need to be realized through inverters, so this kind of energy is called IBR. Compared with traditional synchronous generators, these resources have lower carbon emission, more flexible use and relatively lower cost, but as more and more IBRs are added to the grid, the change of the energy structure and the instability brought by the IBRs bring unprecedented challenges to the frequency control of the power system. In this paper, we will focus on three experiments with microgrids, wind energy and photovoltaic power generation, so as to further understand the differences between the new power generation technologies and the traditional power generation methods.

2. Literature Review

With the wide application of renewable energy in the power system, the role of inverter resources (IBRs) in the grid has gradually become the focus of research. Inverters not only realize the grid integration of renewable energy, but also significantly change the frequency stability and dynamic characteristics of the power system.

2.1. Characteristics of inverter resources (IBR)

An inverter resource is a power electronics-based device whose output frequency is synchronized with the grid frequency, as determined by its internal controller. Compared with conventional synchronous generators, inverters lack inertial reserves, so their dynamic response is faster but their stability is relatively low [1].Droop control, as a strategy that simulates the power distribution characteristics of synchronous generators, is widely used in active and reactive power regulation of microgrids with the advantages of fast response and high adaptability [2].

2.2. Basic theory of microgrid frequency control

Droop control is one of the core technologies of microgrid frequency control, which realizes active and reactive power regulation through the following equations:

$$\Delta f = -k_p \cdot P \tag{1}$$

$$\Delta V = -k_q \cdot Q \tag{2}$$

k_p and k_q are Droop coefficients, which are used to regulate the relationship between active and reactive power and frequency and voltage, respectively. It has been shown that optimizing the Droop coefficient can effectively improve the dynamic performance of microgrids [3,4].

2.3. Power control of doubly-fed induction generator (DFIG)

Doubly-fed induction generator (DFIG) is the mainstream technology of modern wind turbine, which realizes the bidirectional power flow between stator side and rotor side through power electronic converter. The power output of DFIG is closely related to the wind speed and the pitch angle of the blades, and its Maximum Power Point Tracking (MPPT) technology can significantly improve the efficiency of the wind energy utilization [5]. In addition, DFIGs have advantages in fault ride-through (FRT) performance and reactive power support, which contribute to the stability of modern power grids [6].

2.4. MPPT technique for PV inverters

PV inverters maximize the efficiency of solar energy utilization through MPPT algorithms. Current mainstream MPPT algorithms include perturbation observation (P&O) and incremental conductance (IC), both of which exhibit high tracking efficiencies under different irradiance and temperature conditions [7]. It has also been shown that optimizing the control strategy of the inverter can reduce the impact of the PV system on the local grid and improve the quality of the grid-connected voltage [8].

2.5. Power system frequency stability

While conventional synchronous generators maintain grid frequency stability through rotational inertia, inverter resources need to provide frequency support through virtual

inertia (VSG) technology due to the lack of physical inertia. The core of VSG technology lies in the simulation of synchronous generator's dynamic characteristics including inertial response and damping response [9]. Studies have shown that combining the VSG technique with Droop control can further improve the frequency regulation of inverter resources [10].

2.6. Shortcomings and outlook of current research

Most of the existing studies focus on the control strategies of inverter resources and single-scenario experiments, and the research on system-level behaviors under large-scale high-penetration inverter resource conditions is still relatively insufficient. Therefore, in this paper, the performance of Droop control, DFIG and PV inverters in frequency control will be discussed in depth from three experiments of microgrid, wind and PV power generation, so as to provide experimental basis for the frequency stability of future power systems.

3. Research

3.1. Microgrids

Grids with power sources, loads (power consuming equipment) and energy storage units that can be switched to "islanded operation mode" or "grid-parallel operation mode" are called microgrids. This modern power grid system allows for operation on the traditional utility grid as well as self-sufficiency with local power supply. Switching between the two modes of operation usually allows for a seamless transition.

The objective of this study is to investigate the P-droop and Q-droop capabilities of synchronous motors for primary automatic control in isolated microgrids

3.1.1. Equipment

The equipment, part number and designation of microgrids is shown below in Table 1:

Table 1. Microgrids

Equipment	Part Number	Designation
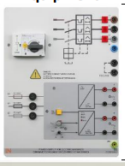	CO3212-5U	Universal Power Supply for DC and Three-Phase Current
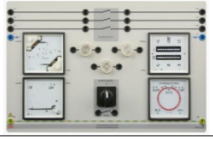	CO3212-6V	Synchronizing Unit
	CO3301-5L	Generator HMI
	CO3636-6W	Servo Machine Test Bench for 1-kW Machines
	CO3301-5G	Exciter Voltage Controller with De-excitation Function
	CO3212-1P	Motor Protection Switch, 3 Pole, 1.6 – 2.5A
	SE2662-5Q	Three-Phase Synchronous Machine with Smooth Core Rotor, 1kW
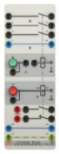	CO3301-5P	Power Switch Module
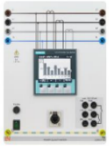	CO5127-1S	Power Quality Meter
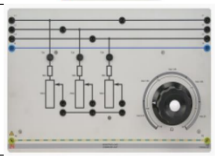	CO3301-3F	Variable Resistor Load, 3-Phase, 1kW
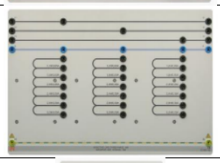	CO3301-3D	Inductive Load, 3-Phase, 1kW
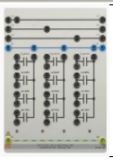	CO3301-3E	Capacitive Load, 3-Phase, 1kW

3.1.2. Wiring Diagram

The wiring diagram of microgrids is shown below in Figure 1:

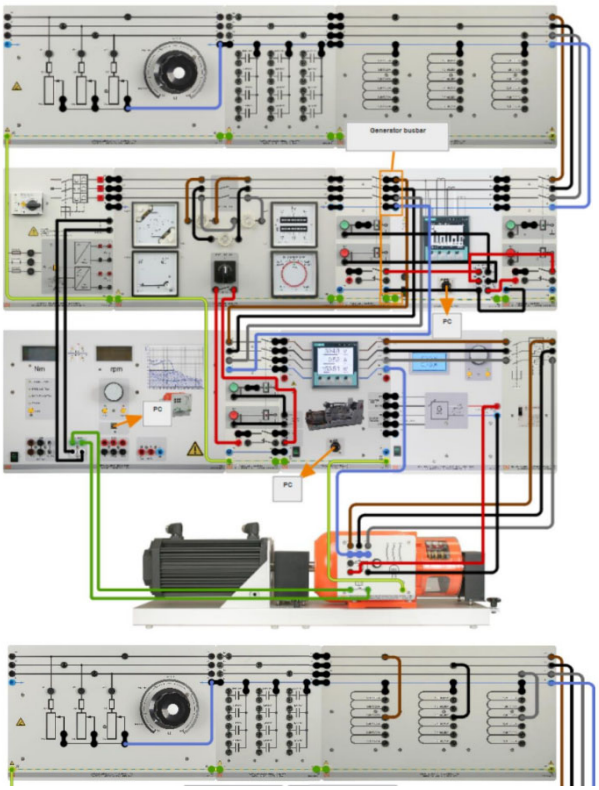

Figure 1. Microgrids

3.1.3. Research Steps

Automatic reactive power control based on Q Droop (with inductive loads)

(1) Open the servo test bench, generator HMI unit, excitation voltage controller and power quality meter.

(2) Open the SCADA viewer from Labsoft

(3) Open the SCADA file

(4) Configure the IP address of the generator HMI and power quality meter in SCADA

(5) Select the Power Quality Meter and click on "Properties". Once a new window opens

(6) Then enter the IP address of the Power Quality Meter, leaving the "Port Number" as 502.

(7) Press the "Run" button in the SCADA toolbar to run SCADA.

(8) In SCADA, set the voltage of the "Master" generator to 400V and the frequency to 50Hz.

(9) Voltage drop is enabled by default, for this activity, set it to 5% as the default setting.

(10) From the "Instrument" menu, turn on the SCADA recorders (1 and 2) to observe and synchronize the display of the motor parameters and record the experimental readings of active power P, reactive power Q, machine voltage U, and the duration of the speed.

(11) Press the "Run Idle" button on the SCADA to start the synchronous machine.

(12) Wait for the synchronous machine to stabilize and reach 1500 rpm.

3.1.4. Results

Table 2. Initial data

Droop Settings (%)	Reference/Previous Voltage (V)	Inductive Load – Q (VAR)	Measured Voltage (V)	Calculated Voltage (V)	Difference (V)
3	400	-247.9	396	396.2815	-0.2815
3	396	0	400	400	0
5	400	-244	394	393.9	0.1
5	394	0	400	400	0
7	402	-241	392	391.565	0.435
7	392	0	400	400	0
9	401	-239.1	391	389.2405	1.7595
9	391	0	400	400	0

Table 3. Automatic reactive power control based on Q Droop (with capacitive loads)

Droop Settings (%)	Reference/Previous Voltage (V)	Capacitive Load – Q (VAR) Measured	Measured Voltage (V)	Calculated Voltage (V)	Difference (V)
3	400	208	404	403.12	0.88
3	404	0	400	400	0
5	400	209	406	405.225	0.775
5	406	0	401	400	1
7	401	212	408	407.42	0.58
7	408	0	401	400	1
9	401	212	409	409.54	-0.54
9	409	0	401	400	1

Table 4. Automatic active power control based on P Droop (with resistive loads)

Droop Settings (%)	Droop Speed (rpm)	Resistive Load – P (W)	Measured Speed (rpm)	Calculated Speed (rpm)	Difference (rpm)	Droop Settings (%)	Droop Speed (rpm)	Resistive Load – P (W)
3	1527.75	0	1544.5	1545	0.5	3	1527.75	0
3	1545	-306	1527.5	1527.78	0.28	3	1545	-306
5	1546	0	1575	1575	0	5	1546	0
5	1575	-306	1546	1546.3	0.3	5	1575	-306

3.1.5. Research Conclusion

Q Droop reactive power control

With inductive loads

The experimental data show that under inductive load conditions, the reactive power is linearly related to the Droop setting. When Droop is increased from 3% to 9%, the deviation of the reference voltage from the measured voltage gradually increases. This is due to the fact that the voltage variation in Droop control is linearly related to the reactive power with the expression:

$$\Delta V = -k \cdot Q \tag{3}$$

where k is the Droop coefficient and Q is the reactive power. Under inductive load conditions, the reactive power is negative and the voltage drop is significant, which indicates that Droop control can effectively limit the voltage instability caused by reactive power under inductive load conditions.

With capacitive load

The experiments with capacitive loads show that as the Droop increases from 3% to 9%, the measured voltage rises gradually, but the deviation is always less than 1 V. This indicates that the positive deviation characteristics of the Droop control are well reflected under capacitive loads. The experiment verifies the adaptability of the Droop control to different load types, and also shows that the voltage compensation effect of the capacitive load can alleviate the grid pressure.

Active Power Control for P Droop

The experimental results show that when Droop is set to 3% and 5%, the speed changes caused by the active power are small, with deviations of 0.5 rpm and 0.3 rpm, respectively, indicating that the Droop control can effectively balance the load fluctuations in islanded operation. The results further support the applicability of Droop control in active power management, especially in the islanded operation mode, where its dynamic response performance is more excellent.

3.2. Wind

This study describes the working principle and function of modern wind turbines doubly fed induction generator (DFIG). Experiments will be conducted to control and observe the active and reactive power distribution of the wind turbine in grid-connected operation. It will also be investigated how the DFIG generator depends on the wind speed at the point of its operating maximum power point (MPP) when supplying power to the grid and the effect of the pitch angle of the paddles on its power output.

3.2.1. Equipment

The equipment, part number and designation of wind is shown below in Table 5:

Table 5. Wind

Equipment	Part Number	Designation
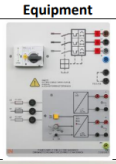	CO3212-5U	Universal Power Supply for DC and Three-Phase Current
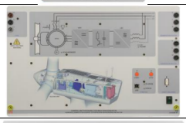	CO3208-3A	Controller for a Wind Power Plant's Doubly-Fed Induction Generator
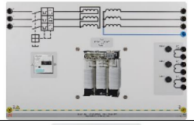	CO3208-3B	Isolating Transformer, 3-Phase, 1-kW
	CO5127-1S	Power Quality Meter
	CO3636-6W	Servo Machine Test Bench for 1-kW Machines
	SE2662-6W	Three-Phase Generator/Motor, 1kW

3.2.2. Wiring Diagram

The wiring diagram of wind is shown below in Figure 2:

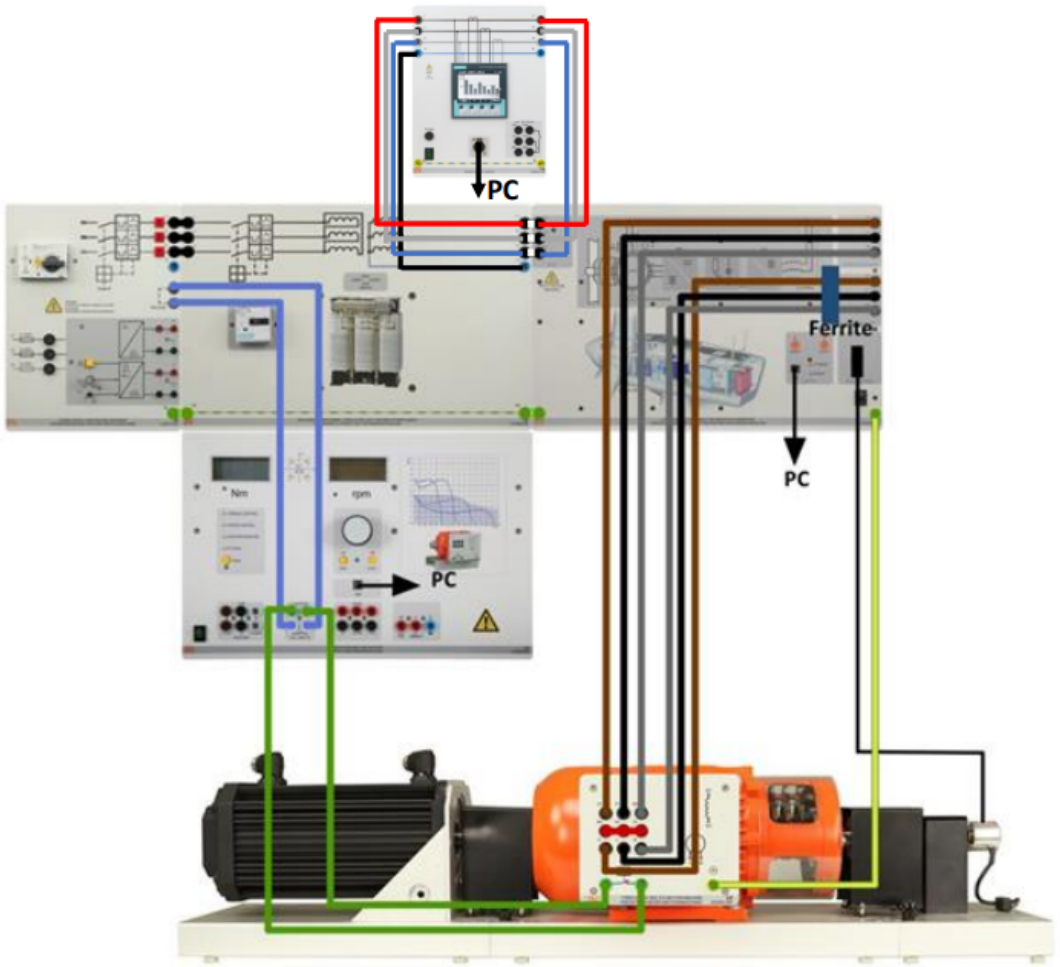

Figure 2. Wind

3.2.3. Research Steps

DFIG active and reactive power control

(1) Open the machine test bench and DFIG control unit

(2) Turn on the power supply (three-phase grid) and make sure that the transformer circuit is normal and the circuit breaker has not tripped.

(3) Open the "Labsoft" software from the "Start Menu".

(4) from the Labsoft "Instrument" menu to open the "Power Control" tool

(5) Select "Stator Power" mode on the virtual instrument.

(6) On the servo base, select "Speed Control" and set the speed to 1200rpm.

(7) Press the "Enable" button on the virtual instrument.

3.2.4. Results

Table 6. Initial data

Speed(rpm)	1200	1250	1300	1350	1400	1450	1500	1550	1600	1650	1700	1750	1800	1850	1900
DFIG (W) Stator Power	400	398	399	398	399	399	398	399	399	397	398	398	398	398	398
LSC (W)	-189	-174	-162	-144	-128	-114	-95	-83	-70	-57	-44	-32	-16	-6	5
Grid (W)	208	223	235	253	269	283	301	314	327	340	353	366	380	391	403

Speed (rpm)	1300	1400	1500	1600	1700	1800
DFIG (W) Stator Power	400	399	398	400	398	398
DFIG (VAR) Stator Power	80	77	80	78	81	78
LSC (W)	-169	-140	-109	-82	-55	-29
LSC (VAR)	0	0	0	0	0	0
Grid (W)	228	256	287	316	342	366
Grid (VAR)	80	79	80	79	77	78

Table 7. Active power control and grid synchronization of DFIG at different wind speeds

Wind Speed (m/s)	Pitch Angle (degrees)	Rotor Speed (rpm)	Torque (Nm)	Pm (W)	Ps (W)	Pr (W)	Pg (W)	Efficiency (%)
3	0	0	0.2	0	0	-20	-20	
3.5	0	875	0.3	25	0	-24	-24	-96
4	0	881	0.5	48	5	-91	-87	-181.25
4.5	0	945	0.7	71	33	-100	-68	-95.77464789
5	0	1038	1	103	55	-104	-48	-46.60194175
5.5	0	1128	1.2	149	78	-104	-25	-16.77852349
6	0	1217	1.4	179	107	-101	3	1.675977654
6.5	0	1301	1.7	226	133	-97	38	16.81415929
7	0	1399	1.9	293	168	-91	77	26.27986348
7.5	0	1499	2.3	355	205	-82	124	34.92957746
8	0	1590	2.5	431	242	-67	176	40.83526682
8.5	0	1684	2.9	523	285	-50	231	44.16826004
9	0	1786	3.3	607	328	-31	300	49.42339374
9.5	0	1879	3.7	715	376	-3	373	52.16783217
10	0	1894	4.1	813	448	6	464	57.07257073
10.5	0	1894	4.7	927	514	24	532	57.38942826
11	0	1897	5.1	997	571	24	598	59.97993982
11.5	0	1899	5.3	1065	614	35	646	60.657277
12	0	1899	6.4	1133	656	39	697	61.51809356
12.5	0	1900	6.1	1197	708	44	746	62.32247285
13	1	1903	6.2	1227	724	47	778	63.40668297
13.5	5	1902	6.1	1242	724	51	776	62.47987118
14	8	1904	6.2	1232	724	54	772	62.66233766

Table 8. Fault ride-through performance of the DFIG

Gain IQ	40% Voltage dip		60% Voltage dip	
	U(g_pos_d)(pu)	I(g_pos_q)(pu)	U(g_pos_d)(pu)	I(g_pos_q)(pu)
0	0.6	0	0.4	0
2	0.6	0.6	0.4	1
3	0.6	0.8	0.4	1.1
4	0.6	1.11	0.4	1.1
6	0.6	1.15	0.4	1.15
8	0.6	1.15	0.4	1.15

3.2.5. Research Conclusion

DFIG active and reactive power control

The experimental results show that the output power of the DFIG increases nearly linearly when the rotational speed is gradually increased from 1200 rpm to 1900 rpm. Specifically, the grid synchronous power increases from 208W to 403W, while the reactive power remains stable. This indicates that modern WTGs have strong stability and power output capability at high rotational speeds. The experimental results also support the theoretical model:

$$P = \omega \cdot T \tag{4}$$

where P is the power, ω is the rotational speed, and T is the torque. As the rotational speed increases, the power increases linearly, verifying the accuracy of the theoretical formula.

Power characteristics at different wind speeds

When the wind speed changes from 3m/s to 14m/s, the system efficiency gradually increases from negative to 62.66%. The low torque and power output under low wind speed conditions even cause negative efficiency, which is due to the fact that the DFIG is difficult to reach the rated speed when the wind speed is insufficient. And when the wind speed exceeds 7 m/s, the system gradually enters the stable output stage, and the power factor and efficiency are significantly improved. This indicates that the DFIG can effectively convert wind energy into electric energy under optimized wind speed, and its performance is closely related to the blade pitch angle and motor speed.

3.3. Photovoltaic

The objective of this study is to investigate the operation and characterization of modern photovoltaic (PV) systems operating under grid coupling.

3.3.1. Equipment

The equipment, part number and designation of photovoltaic is shown below in Table 9:

Table 9. Photovoltaic

Equipment	Part Number	Designation
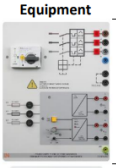	CO3212-5U	Universal Power Supply for DC and Three-Phase Current
	CO5127-1S	Power Quality Meter
	CO3208-1N	3-Phase Industrial Photovoltaic Inverter
	CO3208-1P	Solar Panel Emulator, 1.5kW, 500 V
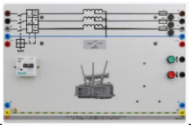	CO3301-3P	Variable 3-Phase Transformer with Motor Drive
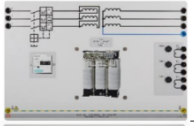	CO3301-3N	Isolating Transformer (1kW) 3-Phase
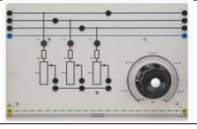	CO3301-3F	Variable Resistor Load, 3-Phase, 1kW

3.3.2. Wiring Diagram

The wiring diagram of photovoltaic is shown below in Figure 3:

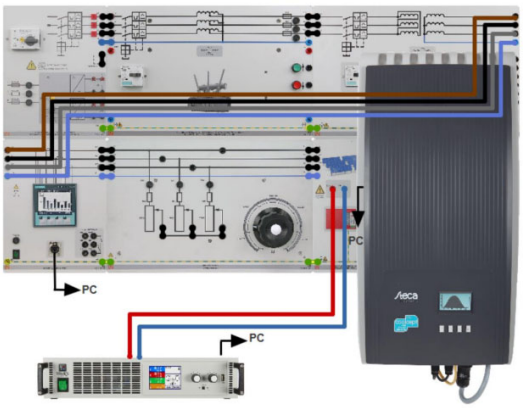

Figure 3. Photovoltaic

3.3.3. Research Steps

Solar PV inverter operating point MPPT (MPP tracking with different irradiance levels)

(1) Turn on the main power supply and the inverter

(2) Set the load resistance to 750 ohms and manually adjust the line-to-neutral voltage to 220V for the local network transformer.

(3) Open “Solar Panel Emulator” hardware.

(4) Open Labsoft's “Solar Panel” virtual tool.

(5) Set SHADOW [%] = 0; SHADED MODULES = 0; IRRADIANCE [%] = 100%.

(6) Press the “Power” button to activate the “Solar Panel Virtual Instrument”.

(7) Wait until the PV inverter tracks its “maximum power point” and synchronizes itself to the grid.

3.3.4. Results

Table 10. Initial data

Irradiance (%)	DC Current (A)	DC Voltage (V)	DC Power (V)	AC Current (A)	AC Voltage (V)	AC Power (V)	Efficiency (%)
100	4.01	359	1439	2.1	221	1388	96.45587213
80	3.16	364	1121	1.7	220	1109	98.92952721
60	2.43	361	878	1.3	220	843	96.01366743
40	1.61	359	576	0.8	220	546	94.79166667
20	0.83	358	288	0.4	220	262	90.97222222
0	0	388	5	0.2	220	0	0

Table 11. Solar PV inverter operating point MPPT (MPPT tracking and shading module)

Shadow (%)	DC Current (A)	DC Voltage (V)	DC Power (V)	AC Current (A)	AC Voltage (V)	AC Power (V)	Efficiency (%)
20	3.5	371	1300	1.9	221	1257	96.69230769
50	3.97	272	1078	1.6	220	1035	96.01113173
80	3.98	271	1080	1.6	220	1035	95.83333333
100	4	270	1080	1.6	220	1035	95.83333333

Table 12. Active power derating and MPP tracking inverter operating point

Active Power Derating in %	P [W] (PV – Inverter)	Calculated P [W] (PV – Inverter)	Difference	P [W] (VLNT)
0	1391	1500	-109	-1093
10	1352	1350	2	-1056
20	1224	1200	24	-925
30	1064	1050	14	-765
40	904	900	4	-604
50	745	750	-5	-441

Table 13. Effect of different irradiance on voltage drop of localized network transformers

Irradiance (%)	Power VLNT (W)	AC Voltage (V)
100	-1169	415
80	-900	406
60	-628	393
40	-357	381
20	-85	366
0	5	351

3.3.5. Research Conclusion

MPPT performance of PV inverters

The PV inverter shows high efficiency under different irradiance. For example, under 100% irradiance, the DC power is 1439W and the AC power is 1388W with an efficiency of 96.45%. As the irradiance decreases to 20%, the efficiency decreases slightly but remains above 90%. This indicates that the MPPT algorithm of the PV inverter has good robustness and can effectively track the maximum power point.

In the partial shadow shading experiment, the DC power loss of the system is less than 15%, e.g., when the shadow covers 50%, the DC power is 1078W and the efficiency is 96%. This indicates that the system can still maintain a high conversion efficiency under partial shading conditions, which verifies the applicability of the PV system in complex lighting environments.

Effect of localized network voltage drop

As the irradiance decreases from 100% to 0%, the local network voltage gradually decreases from 415 V to 351 V. The experimental data show that the PV system is able to provide effective support to the local grid at high irradiance, whereas the grid voltage relies on the support of other power sources when the irradiance decreases. This further illustrates the potential of distributed PV systems in improving grid voltage stability.

4. Analysis of Conclusions

4.1. Utility of Droop control

Whether it is active power or reactive power control, the dynamic response performance of the Droop method in microgrid islanding operation is excellent. Its voltage deviation regulation of inductive and capacitive loads is particularly significant, providing a reliable technical guarantee for the stable operation of islanded microgrids.

4.2. Economy and stability of wind energy system

The experiment verifies the high efficiency of DFIG under high wind speed conditions and shows its power factor regulation capability for the grid, proving that it is suitable for renewable energy deployment in high wind speed areas.

4.3. Adaptability of PV system

The high efficiency and immunity of the PV inverter to different irradiance and shading conditions demonstrate its suitability for complex distributed energy environments. In particular, the high efficiency of the MPPT algorithm provides an important support to further enhance the application scenarios of PV systems.

In this study, the high efficiency and applicability of inverter resource-based power generation technology in modern power systems are verified through an in-depth analysis of three experiments: microgrid, wind and PV. It is shown that the grid's ability to accommodate renewable energy can be significantly enhanced by optimizing the Droop control strategy and improving the efficiency of wind and PV systems. Future research needs to further explore the practical application of these technologies in large-scale power grids to achieve a higher percentage of clean energy integration.

References

[1] Yazdani, A., & Iravani, R. (2010). Voltage-sourced converters in power systems: Modeling, control, and applications. IEEE Press.

[2] Guerrero, J. M., et al. (2007). “A decentralized control strategy for islanded microgrids with renewable energy sources.” IEEE Transactions on Industrial Electronics, 54(2), 899-909.

[3] Katiraei, F., & Iravani, M. R. (2006). “Power management strategies for a microgrid with multiple distributed generation units.” IEEE Transactions on Power Systems, 21(4), 1821-1831.

[4] Lopes, J. A. P., et al. (2006). “Integrating distributed generation into electric power systems: A review of drivers, challenges, and opportunities.” Electric Power Systems Research, 77(9), 1189-1203.

[5] Ackermann, T. (2012). Wind power in power systems. John Wiley & Sons.

[6] Heier, S. (2014). Grid Integration of Wind Energy: Onshore and Offshore Conversion Systems. John Wiley & Sons.

[7] Esram, T., & Chapman, P. L. (2007). “Comparison of photovoltaic array maximum power point tracking techniques.” IEEE Transactions on Energy Conversion, 22(2), 439-449.

[8] Chen, Y., et al. (2014). “Impact of inverter-based distributed generators on local voltage regulation and loss.” IEEE Transactions on Power Systems, 29(1), 95-103.

[9] Driesen, J., & Van Craenenbroeck, T. (2010). “Virtual synchronous generators.” In Proceedings of the IEEE PES General Meeting, 1-3.

[10] Beck, H.-P., & Hesse, R. (2007). “Virtual synchronous machine.” In 9th International Conference on Electrical Power Quality and Utilisation, 1-6.